Geophysica (2026), 61 (1), 3–22

Observed currents from the Gulf of Finland – description of the ADCP dataset (2009–2015)

Hedi Kanarik[1,*,**], *Elina Miettunen*[1,**], *Hanna Berg*[1], *Laura Tuomi*[1], *Pekka Alenius*[1], *and Riikka Hietala*[1]

[1]Finnish Meteorological Institute, P.O. Box 503, FI-00101 Helsinki, Finland
[*]Corresponding author, hedi.kanarik@fmi.fi
[**]Authors contributed equally

(Submitted: 2026-03-31; Accepted: 2026-07-01)

Abstract

The Gulf of Finland (GoF) in the Baltic has been extensively studied for the last three decades. To further support the work in this area, we present the Finnish Meteorological Institute's (FMI's) acoustic Doppler Current profiler (ADCP) dataset from the GoF covering years from 2009 to 2015, published in FMI's Research Data repository. This dataset includes simultaneous measurements from up to three different sites covering ice-free seasons in years 2009–2012 and continuous measurements from April 2013 onwards. In this paper, we give an overall description of the ADCP dataset with detailed information on the metadata and deployment information to facilitate the future use of the measurements. In addition, we present a brief description of the characteristics of the observed currents. The measurements improve understanding of the GoF circulation patterns, showcasing the large variability and vorticity of the currents in the area while catching many events of strong currents due to the relatively long measurement time series.

Keywords: Baltic Sea; ADCP; currents; dataset; Gulf of Finland

1 Introduction

For decades, our understanding of the circulation dynamics in the Gulf of Finland (GoF) relied on the overviews presented by *Witting* (1912) and *Palmén* (1930). These overviews were based on regular current observations from lightships during the open sea season. Their results suggested a resultant cyclonic surface circulation for the GoF. As only a few observation sites were available, the circulation pattern that they estimated was quite coarse. They gave the so-called stability of the currents and noted that it also has considerable seasonal variability. The cyclonic mean circulation is a statistical property, not a prevailing feature, and presenting long-time averages for the GoF hides the variability in the circulation. Later studies based on hydrodynamic modelling (e.g., *Andrejev et al.*, 2004; *Elken et al.*, 2011) also found similar mean circulation pattern, but gave of course a much more detailed picture of the circulation patterns in this area. *Elken et al.* (2003) studied volume transports in the deep layers of the GoF and suggested that the standard estuarine circulation in the GoF with outflow in the upper layer and inflow in the lower layer can occasionally be reversed with strong enough south-westerly winds. This was later confirmed with direct current observations by, e.g., *Liblik et al.* (2013) and *Lips et al.*

(2017). Based on a high-resolution modelling, *Westerlund et al.* (2019) suggested that estuarine circulation and reverse estuarine circulation are roughly as common.

Westerlund et al. (2019) along with other recent model studies (*Maljutenko and Raudsepp*, 2019; *Westerlund et al.*, 2018) have further increased our understanding of the temporal and spatial variability of circulation in the GoF. While these studies had different model resolutions and simulation periods, they found similar features in the surface layer circulation, such as a westward flow along the southern coast of the GoF, which was strongest during spring, and loops or gyres in the western part of the gulf in late summer or autumn. They also showed variability in the location and strength of inflow in the surface layer from the Baltic proper to the GoF, and in the direction and strength of flow along the northern coast.

In winter, the water column in the GoF is well-mixed down to the halocline at depths of 60 m to 80 m, whereas in spring, a seasonal thermocline starts to form and reaches depths of 10 m to 20 m during summer (e.g., *Alenius et al.*, 1998, 2003; *Liblik and Lips*, 2011). Thus, in the central parts of the GoF, where the depth exceeds the depth of the halocline, the water column can have a three-layered structure during the thermally stratified period: an upper layer above the thermocline, a lower layer below the halocline and an intermediate layer between them. In shallower areas, there is a two-layered structure in summer, whereas in winter the water column is mixed down to the bottom. The vertical structure of the currents follows the stratification with opposing current directions in different layers (e.g., *Liblik and Lips*, 2012; *Lilover et al.*, 2017; *Lips et al.*, 2017; *Suhhova et al.*, 2018). Upwelling and downwelling events and reversals of estuarine circulation can occasionally weaken stratification also during summer (e.g., *Liblik and Lips*, 2012).

Different measurement campaigns in the GoF have reported average current speeds of 9 $cm\,s^{-1}$ to 12 $cm\,s^{-1}$ in the upper layer above the thermocline (e.g., *Lilover et al.*, 2017; *Rasmus et al.*, 2015; *Suhhova et al.*, 2018). In coastal areas, current speeds decrease with depth (e.g., *Lilover et al.*, 2017) and, for example, *Rasmus et al.* (2015) reported average current speeds of 4.5 $cm\,s^{-1}$ to 5.0 $cm\,s^{-1}$ near the bottom around 40 m depth in two sites located in the eastern and western GoF close to the northern coast. In deep areas with a three-layer structure in the water column during the seasonally stratified period, the average current speeds are slightly lower in the intermediate layer than in the upper layer and again higher in the bottom layer, 6 $cm\,s^{-1}$ to 13 $cm\,s^{-1}$ (e.g., *Lilover et al.*, 2017; *Suhhova et al.*, 2018). The GoF experiences the strongest tidal oscillation in the Baltic Sea region (*Medvedev et al.*, 2013), and even though tides in the Baltic Sea are relatively weak (*Witting*, 1908, 1910), they are shown to be distinguishable in the GoF (*Lilover*, 2012).

The highest current speeds in the GoF are observed during storms, upwelling and downwelling, as well as during inflow and outflow events. For example, *Liblik and Lips* (2012) reported up to 48 $cm\,s^{-1}$ current speeds both in the upper and deeper layers during inflow and outflow events. *Suhhova et al.* (2018) reported current speeds up to 65 $cm\,s^{-1}$ in the upper layer, up to 51 $cm\,s^{-1}$ in the intermediate layer, and up to 59 $cm\,s^{-1}$ in the bottom layer. *Suursaar and Aps* (2007) reported a coastal jet related to upwelling with near-surface current speeds of up to 60 $cm\,s^{-1}$, while *Lilover et al.* (2025) reported current speeds of up to 70 $\mathrm{cm\,s^{-1}}$ in the intermediate layer during an upwelling event.

In addition to upwelling and downwelling events, eddies and other mesoscale structures are characteristic features in the flow field in the GoF. Such features have been observed both in satellite (e.g., *Kahru et al.*, 1995) and in situ measurements (e.g., *Laanemets et al.*, 2011; *Lips et al.*, 2016; *Pavelson*, 2005) and have also been studied with numerical modelling (e.g., *Väli et al.*, 2017; *Zhurbas et al.*, 2008). Recently, new measuring platforms, such as gliders, and high-resolution modelling have enabled studies on submesoscale variability in stratification and flow field in the GoF (e.g., *Lilover et al.*, 2025; *Salm et al.*, 2025).

Understanding the dynamics of coastal seas and the development of coastal forecasting systems require measurements. Current measurements are much less common than other ocean observations, such as temperature and salinity, and are seldom available in near real time. Furthermore, many existing current measurements from the Baltic Sea are from specific measurement campaigns (e.g. *Green et al.*, 2006; *Kanarik et al.*, 2025; *Liblik et al.*, 2022; *Lilover et al.*, 2017, 2025; *Lips et al.*, 2017; *Muchowski et al.*, 2023; *Rasmus et al.*, 2015; *Suhhova et al.*, 2018, 2015) and are not necessarily openly available.

To advance research and provide data for model development in the GoF, we publish a combined dataset of Acoustic Doppler Current Profiler (ADCP) measurements from the Gulf of Finland in 2009–2015 (*Alenius et al.*, 2026) in FMI's Research Data repository (`https://fmi.b2share.csc.fi/`). These measurements were designed to give background data for surface drift observations that were done in several RV Aranda cruises since 2007. Those drift experiments aimed at understanding of the contributions of different factors that affect the sea surface drift, especially the role of the Stokes drift. The ADCP measurements were done to get data on the differences in current dynamics between the near-coast region and the open sea region. In this paper, we describe the ADCP dataset by *Alenius et al.* (2026) with detailed metadata and deployment information and present an overview of the characteristics of observed currents.

2 *Data description*

The presently published dataset consists of ADCP measurements done on the Finnish side of the GoF in regions roughly between Helsinki archipelago and Juminda peninsula between years 2009 and 2015 (Fig. 2.1, Table 2.1). ADCPs measured simultaneously at three locations, except in 2011, when only two locations had measurements (see Table A1 in Appendix A for details of each deployment). Two of the observation sites (ADCP1 and ADCP2) remained the same throughout the years (Fig. 2.1), while the third site (ADCP3) was changed in 2012 (Fig. 2.1, ADCP3* 2009–2010 and ADCP3 2012–2015). In 2009–2012, measurements were done in the summer season. From April 2013 onwards, continuous measurements are available until December 2014 in ADCP2 and until May 2015 in ADCP1 and ADCP3 sites. The measurement periods for each location are illustrated in Fig. 2.2 with colour indicating the fraction of data disqualified after quality checks. The exact dates of the observation dataset are listed in Table A1.

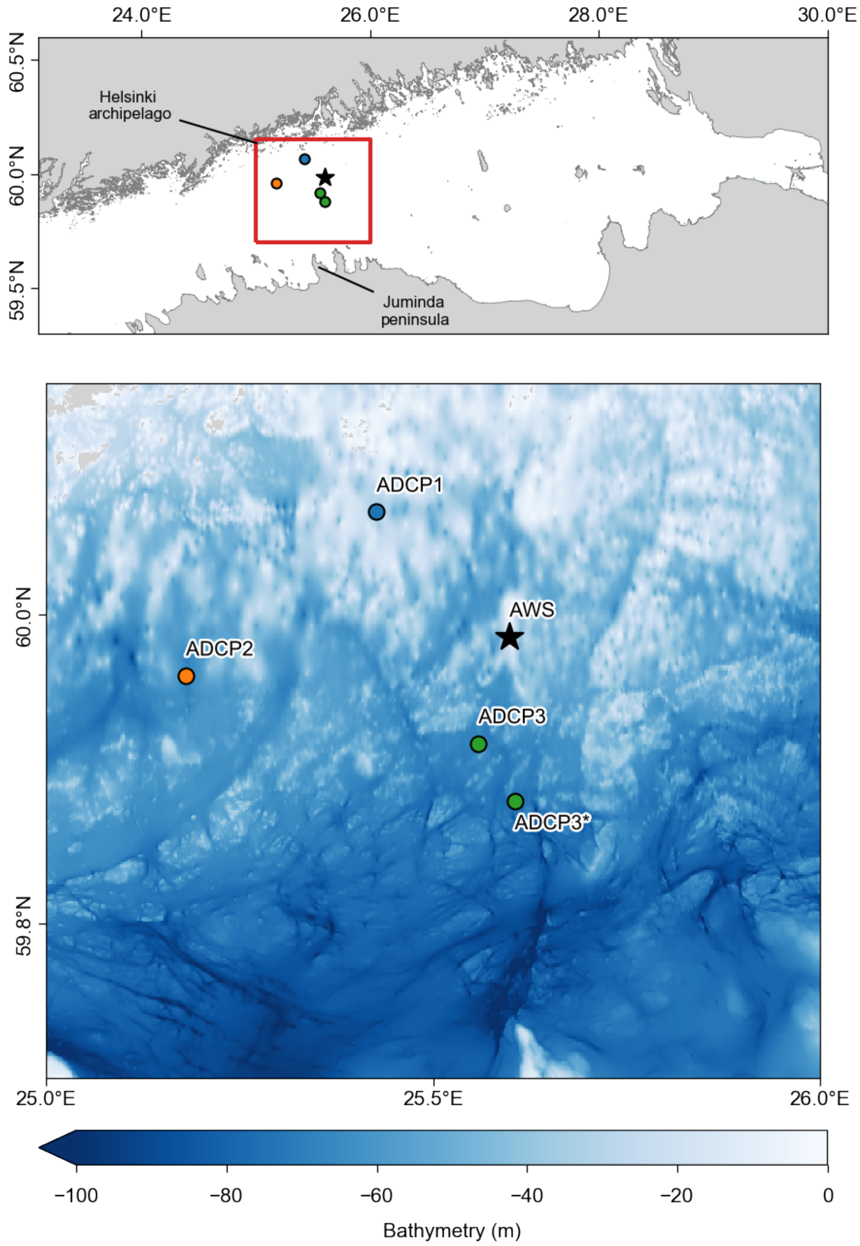

Fig. 2.1: Locations of the ADCP mooring sites in the Gulf of Finland (GoF), indicated with coloured dots. The rectangle in the upper panel indicates the area covered in the detailed map in the lower panel. Location 'ADCP3*' shows the approximate location of the southernmost deployment in 2009 and 2010. The star indicates the location of the Kalbådagrund automatic weather station (AWS). Bathymetry is from *EMODnet Bathymetry Consortium* (2022).

All measurements were performed using Teledyne RD Instruments Workhorse Sentinel ADCP with a 300 kHz device, except for the second dataset in 2013 at ADCP1 measuring between 16 Oct 2013 and 01 Apr 2014 (file `ADCP1_13b`, Table A1), which used the 600 kHz version of Workhorse Sentinel ADCP. The ADCPs were mounted on the bottom, installed on floating buoys anchored to a weight on the sea floor, as presented in the schematic Fig. 2.3. All except the first ADCP1 installation were installed into a spher-

Table 2.1: ADCP moorings published in this paper. The depths were measured with sounding weight during the deployment of each ADCP.

Name	Location	Depth	Number of datafiles
ADCP1	60° 04.000’ N, 25° 25.600’ E	51 m	8
ADCP2	59° 57.630’ N, 25° 10.851’ E	64 m	8
ADCP3	59° 55.000’ N, 25° 33.530’ E	71 m	5
additional measurements:			
ADCP3*$_{2009}$	59° 52.765’ N, 25° 36.327’ E	60 m	1
ADCP3*$_{2010}$	59° 52.775’ N, 25° 36.441’ E	67 m	1

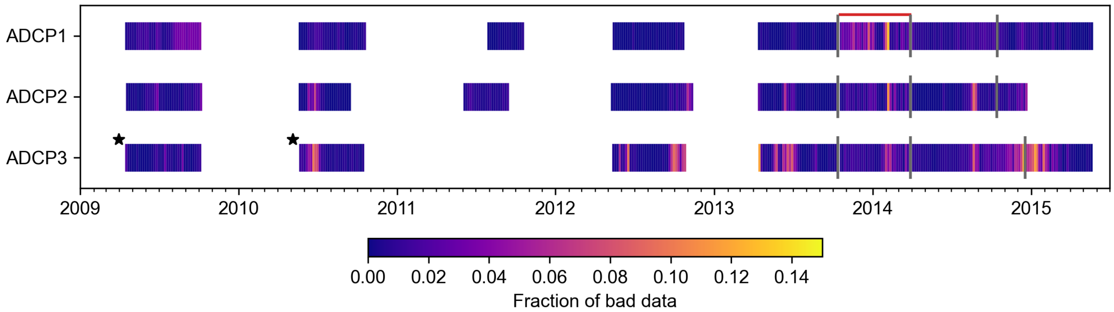

Fig. 2.2: Temporal coverage of the ADCP measurements at each site. The colour shows the fraction of bad data rejected in the quality checks, calculated over all measurement depths in 5 day intervals for illustrative purposes. Grey vertical lines in 2013–2015 indicate the dates when the measurement device was changed. For ADCP1, the red line in winter 2013–2014 outlines the period when the ADCP was deployed at 10 m distance from the bottom and consequently there are no measurements below 39 m depth. For ADCP3, the black stars show the periods when the ADCP was deployed in a different location than in the later years.

ical ADCP buoy (‘orange’ buoy) keeping the device steady also on an uneven seafloor (Fig. 2.3). The first installation of ADCP1 in 2009 was done using a torpedo-like buoy (‘banana’ buoy), which resulted in larger movement of the ADCP and higher error velocities in the observations, and was thus not used in the later installations.

All deployments were set to measure at a half-hour ensemble interval and 1 m bin size. Signals (or pings) are sent evenly over the ensemble interval, and measured values thus represent mean velocities over this half-hour period. The number of pings per ensemble varied between deployments from 135 to 150 and resulted in a variation in standard deviation (`std`) between 1.58 cm s^{-1} to 1.72 cm s^{-1} for the 300 kHz devices and 0.57 cm s^{-1} for the 600 kHz device.

The deployment height (the distance from the sea floor to the ADCP transducers, Fig. 2.3) of each deployment varied from 0.9 m to 1.8 m so that with the blanking zone above the transducers, the first measurement bin was about 4 m to 5 m above the seafloor (1st bin distance from the sea floor, Fig. 2.3). The only exception was the 600 kHz measurements at ADCP1 in 2013, when the ADCP was installed 10 m above the seafloor to ensure that observations could be obtained close to the sea surface. The uppermost measured depth layer varied slightly between the deployments: all deployments in ADCP1 and ADCP3 were able to measure up to 5 m distance from the surface and ADCP2 up to

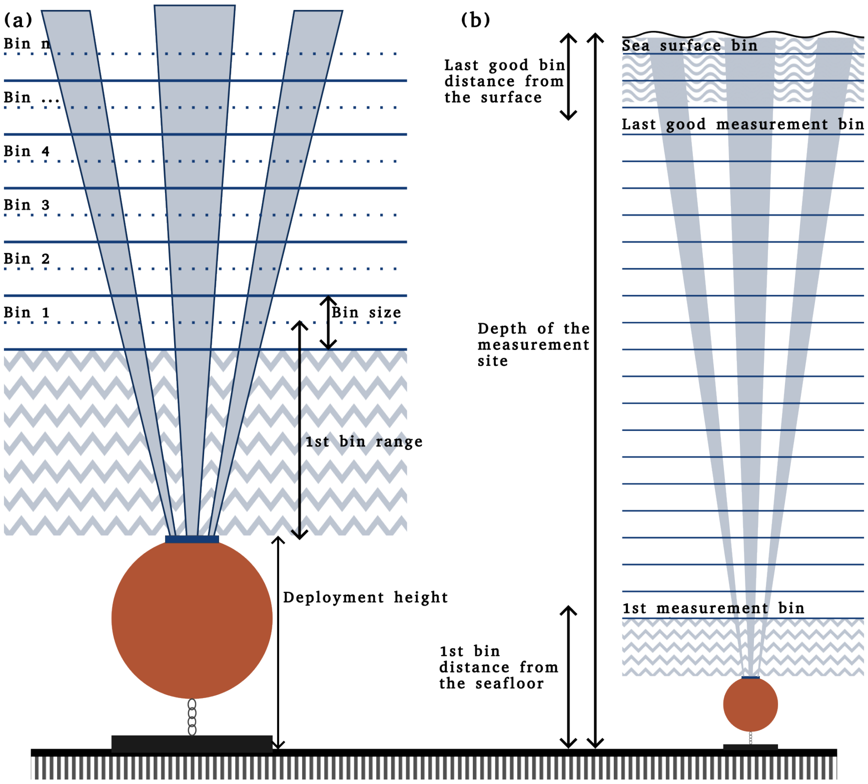

Fig. 2.3: Schematic illustration of ADCP deployment, showing the different depth information given in the metadata. Panel (a) shows details near the bottom, and panel (b) shows the whole water column. The zigzag pattern below the first measurement bin in both panels indicates the blanking zone above the transducers that the device cannot see, and the wavy pattern near the surface in panel (b) indicates the topmost bins that are affected by sidelobe contamination and not included in the dataset. Illustrations are based on *Teledyne RD Instruments* (2011, Figs. 21 and 25).

6 m distance from the surface (Last good bin distance from surface, Fig. 2.3).

2.1 *Datafile structure*

The data from each deployment are included as separate ASCII files in the dataset (*Alenius et al.*, 2026). The files are named with unique deployment IDs that are listed in Table A1. Detailed deployment and configuration information is given in the metadata section at the beginning of each datafile. An example of this metadata section is given in Table 2.2 for one of the deployments. The files include the following variables: the measurement time (in UTC; year, month, day, hours and minutes in separate columns), pressure (`Depth`) measured at the deployment height, magnitude (`Mag`), direction (`Dir`), and u (`U`) and v (`V`) components of the currents at different depth levels or ‘bins’ (`B*`, where `*` stands for the measurement bin number), as shown in Table 2.2.

The metadata row `Original file name` indicates the binary file from which the measurements were extracted using the WinADCP program. The `Device` row provides information on the exact device used and its serial number (SN). The coordinates of each site are given in degrees and their decimals (the exact coordinates are available in Table A1).

The number of bins with good data that determines the number of columns for each variable in the datafile is given by `Number of bins in file`.

In the example given in Table 2.2, there are 55 columns for magnitude, direction, as well as *u* and *v* velocity components, where the column `MagB1` contains the measurements closest to the sea floor and the column `MagB55` contains the ones closest to the sea surface. `Pings/Ens` gives the information of the number of signals used to compute the measured velocities, and `Ensemble interval` tells the time over which the signals were averaged with standard deviation `Std` that is given by the instrument based on the deployment setup. Additionally, metadata includes information on deployment depths and overall data quality, as presented in Sections 2.2 and 2.3.

Table 2.2: An example of the metadata section included at the beginning of each ADCP file (from file `ADCP2_13.csv`; see Table A1 in Appendix A). Lines with metadata start with # sign and the line below them gives the header of the data columns in the file. The first seven columns include the ensemble number (`ens`), year (`YYYY`), month (`MO`), day (`DA`), hours (`HH`) and minutes (`MM`) of the ensemble timestamp in UTC and the measured depth (`Depth`), if available. The rest of the columns include magnitude (`MagB*`, where `*` is the bin number), direction (`DirB*`) and u (`UB*`) and v components (`VB*`) of measured currents. The number of data columns for each variable equals the number of measurement bins in the file.

Variable	Info	Brief explanation for `Info` (not included in the datafile)
`# Original file;`	`AK_2_000.000`	Name of original binary file from which data was extracted using WinADCP program; possible extra identifier in brackets
`# Device;`	`WORKHORSE Sentinel Broadband 307.2 kHz, SN: 13614`	Name of the instrument and serial number of the device
`# Latitude;`	`59.9605`	Latitude converted to decimal degrees
`# Longitude;`	`25.18085`	Longitude converted to decimal degrees
`# Number of bins in the file;`	`55`	Number of depth levels included in the file
`# Pings/Ens;`	`135`	Number of signals used to compute velocities
`# Ensemble interval (s);`	`1800`	Measurement frequency
`# Bin size (m);`	`1`	Size of the depth cell that the measurements represent. Refer to Fig. 2.3
`# 1st bin range (m);`	`2.98`	Blank distance between the ADCP transducers and the first measured bin. Refer to Fig. 2.3.
`# Deployment height (m);`	`0.9`	Distance from the sea floor to the ADCP transducers. Refer to Fig. 2.3.
`# Depth of the measurement site (m);`	`64`	Depth of the site measured during deployment. Refer to Fig. 2.3.
`# Depth measured with;`	`Sounding weight (during deployment).`	Information how `Depth of the measurement site` was determined; can also include information on depth measured with other devices
`# Sea surface around bin;`	`60`	Estimate of ADCP bin at the sea surface. Refer to Fig. 2.3.
`# Std (mm s-1);`	`17.6`	Standard deviation of the measurements, calculated by the device based on deployment setup
`# Units;`	`m (depth), mm s-1 (velocities), deg (direction)`	Units of given variables. All velocities are given as millimeters per second
`# Quality checks done:`		
`#`	`"BIT,Surface side lobe, time, correlation (64), echo intensity (30 db), PG (60%), errorvel (5*std)"`	List of quality checks done and thresholds for disqualifying data. See *Kanarik et al.*, 2018, Section 3, for more details.
`#`	`Bad data (ll>2) marked as; NaN`	Quality flag for marking data as bad and the value used for bad data in this file
`#`	`Notes;`	Notes on the data quality or deployment info; empty if no notable quality issues. See Table A2 for all notes for the whole dataset.
`# Data originator;`	`Finnish Meteorological Institute`	Producer and owner of the data
`# DOI;`	`10.57707/fmi-b2share.n91q0-vms10`	Unique identifier of the dataset
`ens; YYYY; MO; DA; HH; MM; Depth;MagB1;...;MagB55; DirB1;...;DirB55; UB1;...;UB55; VB1;...;VB55`		Columns in the file. In this example, there are 55 columns for each variable (magnitude, direction and u and v components).

2.2 *Determining measurement depths from metadata information*

The vertical extent of each measurement bin is given as `Bin size` in the metadata. To calculate the depth for an individual bin, one needs to account for the ADCP distance from the sea floor (Deployment height) and the distance of the first bin from the transducer (1^{st} bin range) as well as the `Depth of the measurement site` to convert the distance of each bin from the sea floor to the actual depth from the sea surface (Fig. 2.3). The distance from the seafloor for a given bin can be calculated as follows: `Deployment height (m)` + `1st bin range (m)` + (bin number – 1) · `Bin size (m)`. To convert this to the actual depth from the sea surface, use the deployment height information as follows: `Depth of the measurement site (m)` – `Deployment height (m)` – `1st bin range (m)` – (bin number – 1) · `Bin size (m)`. For example, for the fifth bin (B5) in the file in Table 2.2 the distance from the seafloor would then be $0.9\,\mathrm{m}+2.98\,\mathrm{m}+(5-1)\cdot 1\,\mathrm{m} = 7.88\,\mathrm{m} \approx 8\,\mathrm{m}$, and the distance from the sea surface would be $64\,\mathrm{m}-0.9\,\mathrm{m}-2.98\,\mathrm{m}-(5-1)\cdot 1\,\mathrm{m} = 56.12\,\mathrm{m} \approx 56\,\mathrm{m}$. In case the datafile includes the pressure measured by the device itself, the distance from the sea floor can be calculated using the 'Depth' column: `Depth (m)` – `1st bin range (m)` – (bin number – 1) · `Bin size (m)`. This method also accounts for the temporal variation of sea level above the ADCP. Refer to Fig. 2.3 for details on the different depths given as part of the metadata in each file (example in Table 2.2). The bin depth calculated using the 1^{st} bin range gives the depth at the middle of the bin.

Usually, the `Depth of the measurement site` was determined with a sounding weight by the marine observation technicians, but in some cases, acoustic sounding instruments were used. The metadata column `Sea surface around bin` (see 'Sea surface bin' in Fig. 2.3) is included to help determine the distance from the sea surface in case there was no pressure sensor on the ADCP. The depth of the topmost bin can be roughly calculated as the `Sea surface around bin` minus the `Number of bins in the file`, meaning that in the example case, `MagB55` values represent current magnitudes at 5 m depth. The `Notes` row includes information on whether the ADCP had a pressure sensor and whether it was functioning correctly. Even though we give the depth measured by the ADCP's pressure sensor as part of the dataset, there were no proper quality checks made to these depth measurements. The ADCP pressure sensor can experience drifting, causing errors in the depth values, and only very obvious and strong drifts were flagged as bad. More subtle cases of drifts in depth values are most likely present in the published dataset. Unfortunately, for some deployments, the metadata were incomplete, so we used expert judgement in determining the deployment depths. The affected deployments are listed in Table A2 in Appendix A. The metadata `Notes` for each file include this information along with more detailed descriptions of the assumptions made.

2.3 *Quality control performed to the dataset*

Quality control was applied to the data using internal ADCP quality parameters: signal correlation, echo intensity, percent good, and error velocity. Magnetic deviation was corrected before deployment by field technicians by calibrating compasses and applying up-to-date magnetic declination correction. In addition, checks were done to remove depth layers affected by sidelobe contamination (topmost bins), as well as the deployment times and overall device health (BIT number). Following the recommendations of *Book et al.* (2007) and *Symonds* (2006), data were rejected according to these rules: (1) the correlation of signals dropped below 64, (2) the percentage of signals that were usable for velocity computation was below 60% (PG), (3) echo intensity experienced spikes over 30 dB, and (4) the measured error velocity exceeded five times the standard deviation that is calculated by the instrument based on deployment setup (`Std` in Table 2.2). A more detailed description of the procedure is given in *Kanarik et al.* (2018, Section 3). If there was a considerable amount of rejected data, it is mentioned in the `Notes` row of the metadata section, with description of the main reason for the data rejection in each case. Reasons for data rejection include, for example, cases when the deployment experienced large movement that reduced data quality near the surface, and interference from ice during winter. All these notes are collected in Table A2 to provide users with a better overall view on possible data issues. The data files include only data with a good quality flag, and data with any other quality flags were excluded, represented as missing values in the data file. The amount of data rejected is also visualised in Fig. 2.2. We checked ice chart data (*Eriksson et al.*, 2025) for the measurement periods, and ice was present at ADCP1 and ADCP2 locations only during February 2014. During ice-covered times, we only had good measurements from the bottom half of the water column (up to bin 15) from ADCP1 (File ID `ADCP1_13b` in Table A1 and A2).

The complete dataset, including flagged measurements, quality flags, and quality parameters as well as vertical velocities is available on request from the authors. There are large uncertainties related to the measured vertical velocities due to zooplankton and its movement in the water column (*Karvo*, 2023). As our quality control procedures cannot take this into account, we decided not to include vertical velocities in the distributed data.

2.4 Atmospheric data

To present the wind conditions in the GoF close to the ADCP locations, we used measured winds at 32 m height from Porvoo Kalbådagrund automatic weather station (AWS) located at 59° 59' 8.46" N, 25° 35' 55.64" E (Fig. 2.1). Winds are 10-minute average values. The measurements are openly available from the FMI's open database (FMI; `https://en.ilmatieteenlaitos.fi/open-data`, last access: 31 March 2026).

2.5 CTD data

To complement the ADCP dataset, we also publish CTD profiles measured at the time of deployment and occasionally also at the time of retrieval of the ADCP. CTD measurements were performed using vessel-mounted SBE911+ instrument by Sea-Bird onboard RV Aranda close to each ADCP deployment site.

This dataset is collected into the `CTD_dataset.zip` file in *Alenius et al.* (2026) that includes altogether 27 `cnv` files: 10 profiles at ADCP1 and ADCP2, and 7 profiles at ADCP3. The files are named as `CTD_adcpSiteName_YearMonthDay.cnv`, for example `CTD_ADCP1_20090414.cnv`.

3 Characteristics of the observed currents

We present an overview of the currents at the three measurement locations, ADCP1, ADCP2 and ADCP3 (locations shown in Fig. 2.1). Measurements from the location ADCP3*, only covering 2009 and 2010, were excluded from the analysis because it is located too far from ADCP3 to be considered the same measurement station (Fig. 2.1). The presented data include six summers for ADCP1 and ADCP2, and four for ADCP3. In addition, there are data from two winters for ADCP1 and ADCP3, and one for ADCP2. In winter 2013–2014, the data from ADCP1 do not include the lowest part of the water column (below 39 m depth) due to the different deployment depth (see File ID `ADCP1_13b` in Table A2).

The currents at ADCP1 are oriented east-west throughout the water column following the orientation of the coastline (Fig. 3.1a,d,g). ADCP2 (Fig. 3.1b,e,h) and ADCP3 (Fig. 3.1c,f,i) are located farther away from the coast, and the surface layer currents have a wider directional distribution compared to ADCP1. At both locations, there are slightly more currents towards the east and west than towards the north and south. The strongest currents in the surface layer (magnitudes greater than 30 $\mathrm{cm\,s^{-1}}$) flowed most commonly towards the east in ADCP1 and ADCP2, following the direction of the strongest winds at the Kalbådagrund automatic weather station (Fig. 3.2), but this distribution of strong currents was less prominent in ADCP3 measurements. The currents in the bottom layer are oriented along the bathymetry, and the directions alternate dominantly between NNE and SSW at ADCP2 (Fig. 3.1e) and between ENE and WSW at ADCP3 (Fig. 3.1f). At both locations, the currents start to orient along the bathymetry at 15 m or less above the seafloor.

Measured currents are strongest in the surface layer, where the mean current speeds are 10–12 $\mathrm{cm\,s^{-1}}$ and the medians are 9–11 $\mathrm{cm\,s^{-1}}$ (Table 3.1). In the bottom layer, the mean and median current speeds are roughly half of those in the surface layer. Most of the time, currents do not exceed these mean values by much as the 90^{th} percentile for the whole water column is approximately 13–14 $\mathrm{cm\,s^{-1}}$ (Table 3.1). The distributions of the ADCP magnitudes at the three locations with simultaneous measurements (Fig. 3.3) from 12 April 2013 to 27 December 2015 show that, in general, the station closest to the coast (ACDP1) has the highest occurrence of lower current speeds, whereas the currents are slightly stronger in the stations farther from the coast (ADCP2 and ADCP3). The tail of the distributions is very long, with all stations having measured currents up to 70 $\mathrm{cm\,s^{-1}}$. However, currents of over 45 $\mathrm{cm\,s^{-1}}$ have occurrence below 0.0001 (not shown) and are very sensitive to the amount of missing data that is different in each dataset (see Fig. 2.2).

Maximum current speeds, up to 70 $\mathrm{cm\,s^{-1}}$ to 74 $\mathrm{cm\,s^{-1}}$ in the surface layer, occurred during different autumn storms. The maximum values at ADCP1 were measured on 5 Oct 2013 (Fig. 3.4a), at ADCP2 on 3 Nov 2014 (Fig. 3.4b), and at ADCP3 on

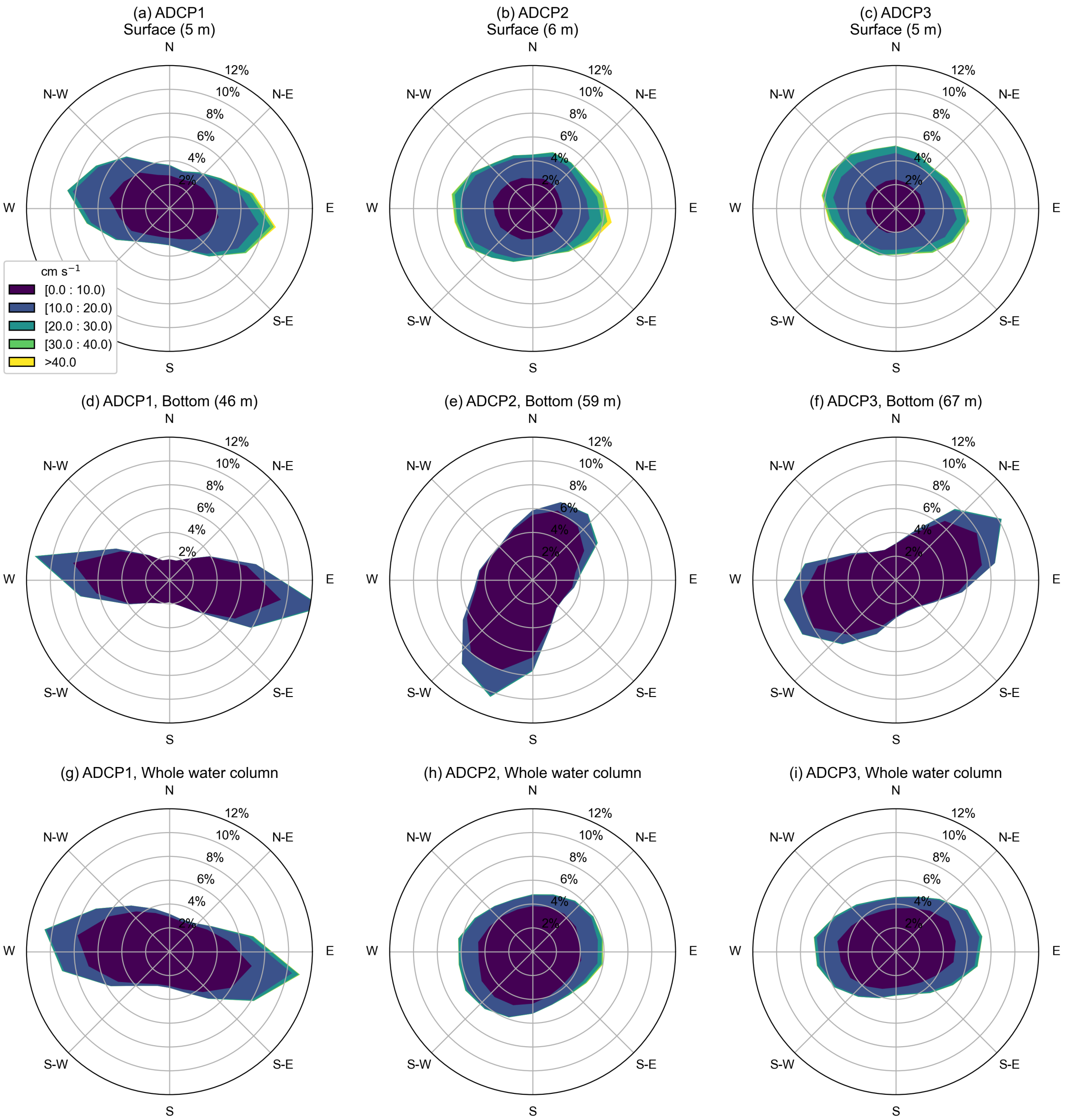

Fig. 3.1: Current roses drawn with all data from surface (first row) and bottom (second row) layers and from the whole water column (last row) at ADCP1 (left panels), ADCP2 (middle) and ADCP3 (right). Data for ADCP1 did not include measurements below 39 m depth in winter 2013–2014 (see Fig 2.2). Years 2009 and 2010 are not included in the roses of ADCP3. Direction distribution shows the direction where the currents are flowing to.

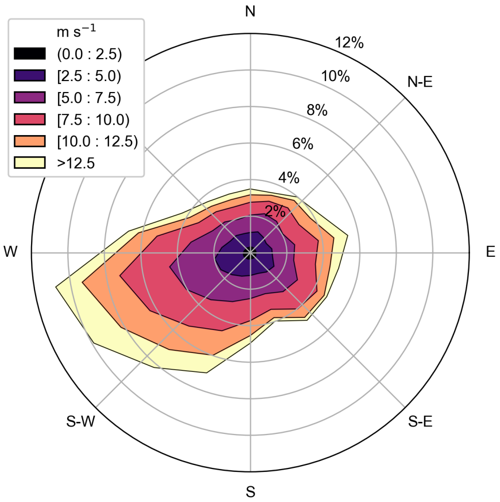

Fig. 3.2: Winds at Kalbådagrund automatic weather station 2009–2025, direction distribution shows the incoming wind direction.

Table 3.1: Statistics of current magnitudes (cm s^{-1}), calculated over all measurement periods at each site. P90 and P99 are the 90th and 99th percentiles, respectively. Data for ADCP1 did not include measurements below 39 m depth in winter 2013–2014 (see Fig. 2.2). Years 2009 and 2010 are not included in the statistics of ADCP3.

Location	Layer	Mode	Median	Mean	P90	P99	Max
ADCP1	Surface (5 m)	6	9	10	19	34	71
ADCP1	Bottom (46 m)	3	5	6	11	18	32
ADCP1	All depths	4	6	7	13	24	74
ADCP2	Surface (6 m)	6	10	11	21	37	72
ADCP2	Bottom (59 m)	3	4	5	10	17	36
ADCP2	All depths	4	6	7	14	25	72
ADCP3	Surface (5 m)	6	11	12	23	35	67
ADCP3	Bottom (67 m)	3	5	5	10	18	35
ADCP3	All depths	4	7	8	14	25	72

10 Nov 2013 (Fig. 3.4c). The direction of the strongest currents was towards east during all these events. Here we discuss these events shortly, to highlight the large spatial variability between the three measurement locations and the type of the most extreme measurements from each station. In Fig. 3.4 we show currents measured at 10 m depth, because the bins closer to the surface contained more missing values during these events.

On 5 Oct 2013, the AWS at Kalbådagrund measured wind speeds of up to 15 m s^{-1}, first from westerly direction and turning later on to south-westerly direction (not shown). The current direction in the upper 20 m layer at ADCP1 was eastward and the current magnitude started to increase on 4 Oct, fluctuating between 20–50 cm s^{-1}. In the evening of 5 Oct the current magnitude relatively quickly increased to the maximum value of 74 cm s^{-1} at 5 m depth at ADCP1. Simultaneously, ADCP2 and ADCP3 measured currents up to 30 cm s^{-1} magnitudes in the upper 20 m layer (not shown). The currents were mostly aligned towards east at ADCP3 and towards north at ADCP2.

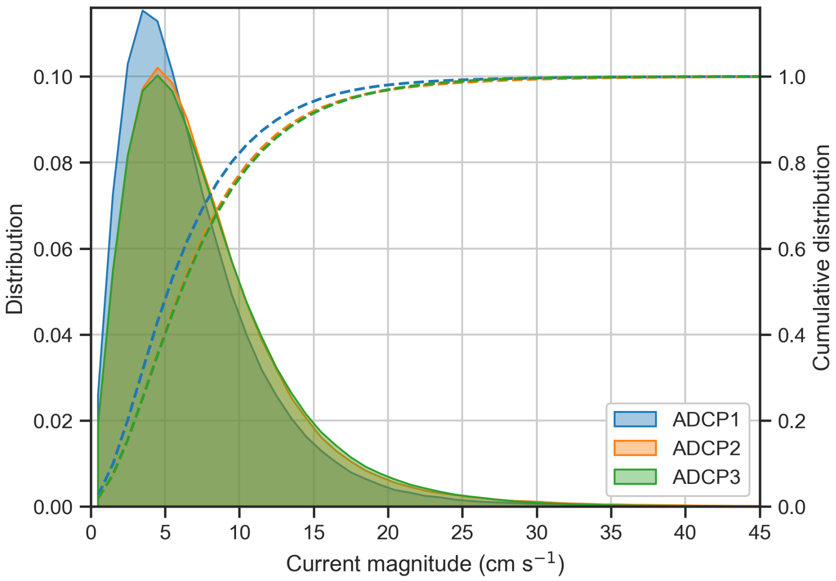

Fig. 3.3: Histograms of current magnitudes calculated for the period from 12 Apr 2013 to 27 Dec 2014. Measurements at ADCP1 did not include data below 39 m depth in winter 2013–2014 (see Fig 2.2). Distribution (left vertical axis, filled lines) is calculated with 1 cm s^{-1} bin size and it is presented as fractions of the whole dataset together with cumulative distributions (right vertical axis, dashed lines). The distribution of the currents exceeding 45 cm s^{-1} is not shown; maximum current speeds reach up to 70 cm s^{-1} but the probability distribution for currents over 50 cm s^{-1} is less than 5×10^{-5}.

In the beginning of Nov 2014 winds slowly increased from 5 m s^{-1} to 10 m s^{-1} to 15 m s^{-1} while turning from northerly direction on 1 Nov to south-westerly by noon of 2 Nov. ADCP2 measured eastward currents in the upper 30 m layer, reaching maximum magnitudes of 72 cm s^{-1} at 5 m depth on 3 Nov 2014 (Fig. 3.4b). At the same time, ADCP3 measured only slightly lower currents flowing towards the south and south-east, whereas ADCP1 measured currents towards the east with magnitudes well below 20 cm s^{-1}.

On 9–10 Nov 2013, all three ADCPs measured short eastward event in the upper 20 m layer, with the current magnitudes exceeding 20 cm s^{-1} for approximately 6 (ADCP1, not shown) to 9 hours (ADCP3, Fig. 3.4c). This event was preceded and followed by weaker westward currents. Winds before the event suddenly turned from south-westerly 10 m s^{-1} to south-easterly that reached 16 m s^{-1}. ADCP1 measured the weakest currents that increased to a bit more than 30 cm s^{-1}, at ADCP2 currents reached around 40 cm s^{-1} whereas at ADCP3 the eastward flow reached around 72 cm s^{-1} at 5 m depth.

Modelling in the GoF region has showcased the presence of circulation patterns with large spatial variation in current magnitudes and directions, featuring strong flow in some areas and weaker flow in others (*Westerlund et al.*, 2019). Looking at the single events from three simultaneous measurements shows the spatial variability within the measurement area and gives a hint on different mesoscale features, such as eddies. However, measurements from couple of locations alone cannot give an overview of the circulation of the entire GoF. Hydrodynamic models, in turn, provide a basin-wide coverage and they can be useful for studying circulation especially when the model results can be verified by a sufficient amount of good quality measurements. The presented high-current event observed

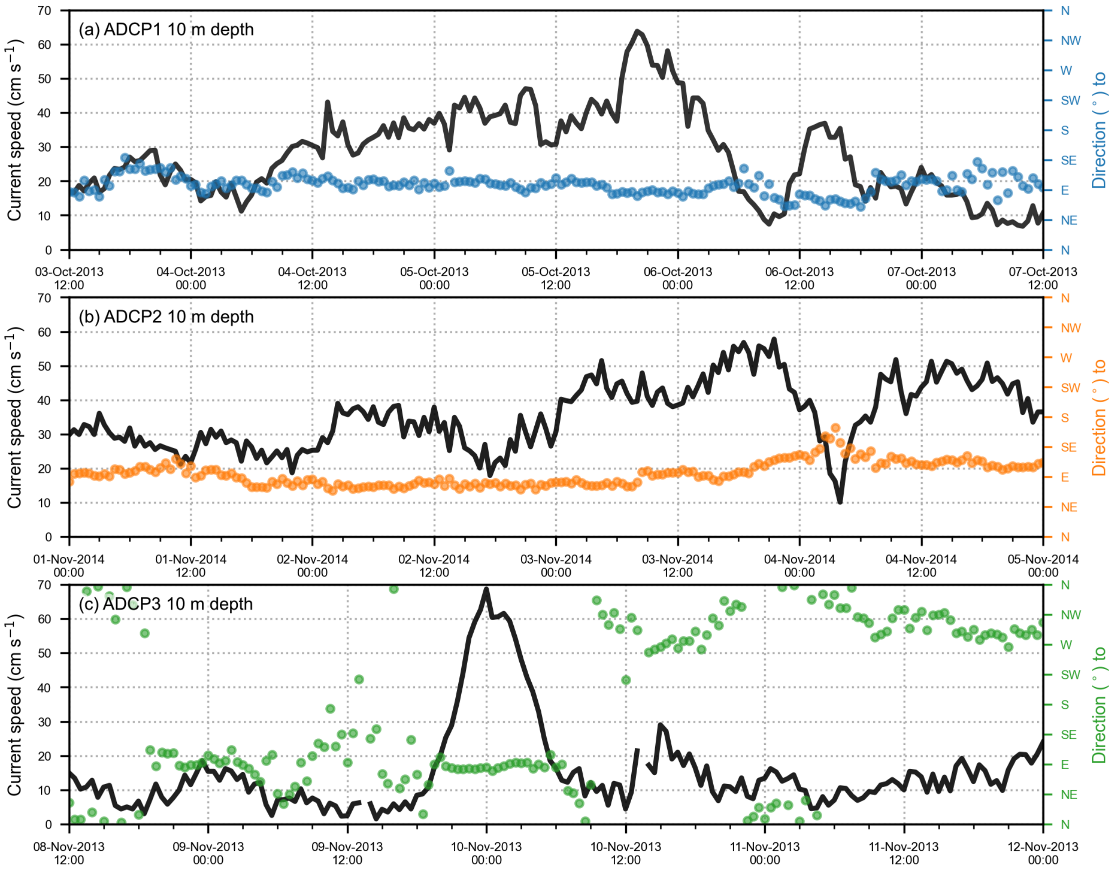

Fig. 3.4: Time series of current magnitude and direction at 10 m depth before, during and after the three different events of strong currents: (a) ADCP1 in 3–7 October 2013, (b) ADCP2 in 1–5 November 2014, and (c) ADCP3 in 8–11 November 2013.

on 5 Oct 2013 displayed features typical of a coastal jet, whereas the other two events likely displayed different features, such as south-north meandering currents [shown, for example, in the works by *Salm et al.* (2025, Fig. 8b) and *Westerlund et al.* (2019, Fig. 9c)].

4 *Summary*

Here, we present a dataset of simultaneous ADCP measurements from three different locations in the Gulf of Finland (Fig. 2.1 and Table 2.1). Data are available from late spring to mid-autumn from 2009 to 2012 and continuously from April 2013 to December 2014 or to May 2015 depending on the location (Fig. 2.2). Measurements were done using bottom-mounted Teledyne RD Instruments Workhorse Sentinel ADCPs, with most of the measurements covering the water column from approximately 5 m below the surface to 5 m above the seafloor in 1 m vertical resolution (see example of the mooring in Fig. 2.3).

The measurements show that the currents at the station closest to the coast are strongly oriented along the coast, whereas the currents at the stations farther offshore show prominent orientation only in deeper layers where they are bound by bathymetric features (Fig. 3.1). The mean current speed through the whole water column varied between $7\,\mathrm{cm\,s^{-1}}$ to $8\,\mathrm{cm\,s^{-1}}$, and 99 percent of the measured current speeds remained below $24\,\mathrm{cm\,s^{-1}}$ to $25\,\mathrm{cm\,s^{-1}}$ (Table 3.1).

The dataset, *Alenius et al.*, 2026, is openly available through Finnish Meteorological Institute's data repository (`https://fmi.b2share.csc.fi/`). Detailed description of metadata is given in Section 2.1 with an example in Table 2.2. The exact filenames and measurement durations for each deployment and description of data issues can be found in Tables A1 and A2 in Appendix A.

Author contributions

The work for publishing and describing this ADCP dataset from the GoF region was initiated by L. Tuomi and H. Kanarik. P. Alenius and R. Hietala planned the original measurement campaigns. H. Berg performed the quality control and initial analysis with the support of H. Kanarik. H. Kanarik wrote the description of the dataset with metadata information and quality control procedures. E. Miettunen and H. Kanarik performed the final analysis of the current conditions. All authors contributed to writing this article.

Acknowledgement

The measurements have been conducted by the Finnish Meteorological Institute during 2009–2015. The original motivation for the measurements was to collect longer time series data on the currents as a background information for several short term surface drift experiments that were done during RV Aranda cruises.

We thank all the researchers and technicians that have taken part in the planning of the measurement campaigns, deployments and recoveries of the measurement equipment and processing of the data. The writing of this paper and publishing of the dataset was supported by CoWup project funded by the Strategic Research Council of Finland (grant no. 365488).

References

Alenius, P., R. Hietala, H. Berg, H. Kanarik, H. Jalli, T. Purokoski, P. Kosloff and T. Roine, 2026. *FMI Gulf of Finland ADCP datasets (2009–2015) [Data set]*. Finnish Meteorological Institute. DOI: `10.57707/fmi-b2share.paypq-7gw46`.

Alenius, P., K. Myrberg and A. Nekrasov, 1998. The physical oceanography of the Gulf of Finland: a review. *Boreal Environment Research*, **3**, 97–125.

Alenius, P., A. Nekrasov and K. Myrberg, 2003. Variability of the baroclinic Rossby radius in the Gulf of Finland. *Continental Shelf Research*, **23** (6), 563–573. DOI: `10.1016/S0278-4343(03)00004-9`.

Andrejev, O., K. Myrberg, P. Alenius and P. A. Lundberg, 2004. Mean circulation and water exchange in the Gulf of Finland—a study based on three-dimensional modelling. *Boreal Environment Research*, **9** (1). URL: `https://www.borenv.net/BER/archive/pdfs/ber9/ber9-001.pdf`.

Book, J. W., H. Perkins, R. P. Signell and M. Wimbush, 2007. The Adriatic Circulation Experiment Winter 2002/2003 Mooring Data Report: A Case Study in ADCP Data Processing. Tech. rep. (last access: 3 Nov 2025). DTIC Document. URL: https://apps.dtic.mil/sti/html/tr/ADA469990/.

Elken, J., M. Nõmm and P. Lagemaa, 2011. Circulation patterns in the Gulf of Finland derived from the EOF analysis of model results. *Boreal Environment Research*, **16** (suppl. A), 84–102.

Elken, J., U. Raudsepp and U. Lips, 2003. On the estuarine transport reversal in deep layers of the Gulf of Finland. *Journal of Sea Research*, **49** (4), 267–274. DOI: 10.1016/S1385-1101(03)00018-2.

EMODnet Bathymetry Consortium, 2022. *EMODnet Digital Bathymetry (DTM 2022)*. DOI: 10.12770/ff3aff8a-cff1-44a3-a2c8-1910bf109f85.

Eriksson, P. B., J. Vainio, N. Tollman, A. Jokiniemi, A. Arola, M. Mäkynen, J. Karvonen and A. Kangas, 2025. The Finnish Ice Service, its sea-ice monitoring of the Baltic Sea and operational concept. *Frontiers in Marine Science*, **Volume 12 - 2025**. DOI: 10.3389/fmars.2025.1561461.

Green, M., B. Liljebladh and A. Omstedt, 2006. Physical oceanography and water exchange in the Northern Kvark Strait. *Continental Shelf Research*, **26** (6), 721–732. DOI: 10.1016/j.csr.2006.01.012.

Kahru, M., B. Håkansson and O. Rud, 1995. Distributions of the sea-surface temperature fronts in the Baltic Sea as derived from satellite imagery. *Continental Shelf Research*, **15** (6), 663–679. DOI: 10.1016/0278-4343(94)E0030-P.

Kanarik, H., L. Tuomi, P. Alenius, M. Lensu, E. Miettunen and R. Hietala, 2018. Evaluating Strong Currents at a Fairway in the Finnish Archipelago Sea. *Journal of Marine Science and Engineering*, **6** (4). DOI: 10.3390/jmse6040122.

Kanarik, H., L. Tuomi, P. Alenius, E. Miettunen, M. Johansson, T. Roine, A. Westerlund and K. K. Kahma, 2025. Currents and their drivers in the Archipelago Sea: insights from ADCP measurements. *Ocean Science*, **21** (5), 2125–2147. DOI: 10.5194/os-21-2125-2025.

Karvo, S., 2023. "Using acoustic current measurements in zooplankton research in the Baltic Sea". (last access: 27 June 2025). MA thesis. University of Helsinki, Finland. URL: http://hdl.handle.net/10138/565797.

Laanemets, J., G. Väli, V. Zhurbas, J. Elken, I. Lips and U. Lips, 2011. Simulation of mesoscale structures and nutrient transport during summer upwelling events in the Gulf of Finland in 2006. *Boreal Environment Research*, **16** (A), 15–26.

Liblik, T., J. Laanemets, U. Raudsepp, J. Elken and I. Suhhova, Oct. 2013. Estuarine Circulation Reversals and Related Rapid Changes in Winter Near-Bottom Oxygen Conditions in the Gulf of Finland, Baltic Sea. *Ocean Science*, **9** (5), 917–930. DOI: 10.5194/os-9-917-2013.

Liblik, T. and U. Lips, 2011. Characteristics and variability of the vertical thermohaline structure in the Gulf of Finland in summer. *Boreal Environment Research*, **16** (suppl A.), 70–83.

Liblik, T. and U. Lips, 2012. Variability of synoptic-scale quasi-stationary thermohaline stratification patterns in the Gulf of Finland in summer 2009. *Ocean Science*, **8** (4), 603–614. DOI: 10.5194/os-8-603-2012.

Liblik, T., G. Väli, K. Salm, J. Laanemets, M.-J. Lilover and U. Lips, 2022. Quasi-steady circulation regimes in the Baltic Sea. *Ocean Science*, **18** (3), 857–879. DOI: 10.5194/os-18-857-2022.

Lilover, M.-J., 2012. "Tidal currents as estimated from ADCP measurements in "practically non-tidal" Baltic Sea". In: *2012 IEEE/OES Baltic International Symposium (BALTIC)*, 1–4. DOI: 10.1109/BALTIC.2012.6249181.

Lilover, M.-J., J. Elken, I. Suhhova and T. Liblik, 2017. Observed flow variability along the thalweg, and on the coastal slopes of the Gulf of Finland, Baltic Sea. *Estuarine, Coastal and Shelf Science*, **195**, 23–33. DOI: 10.1016/j.ecss.2016.11.002.

Lilover, M.-J., U. Lips, T. Liblik, I. Suhhova and G. Väli, 2025. Variability of stratification and currents at the submesoscale detected from CTD and current profiles in the central Gulf of Finland. *Boreal Environment Research*, **30**. DOI: 10.60910/ber2025.jtg5-j683.

Lips, U., V. Kikas, T. Liblik and I. Lips, 2016. Multi-sensor in situ observations to resolve the sub-mesoscale features in the stratified Gulf of Finland, Baltic Sea. *Ocean Science*, **12** (3), 715–732. DOI: 10.5194/os-12-715-2016.

Lips, U., J. Laanemets, I. Lips, T. Liblik, I. Suhhova and Ü. Suursaar, 2017. Wind-driven residual circulation and related oxygen and nutrient dynamics in the Gulf of Finland (Baltic Sea) in winter. *Estuarine, Coastal and Shelf Science*, **195**, 4–15. DOI: 10.1016/j.ecss.2016.10.006.

Maljutenko, I. and U. Raudsepp, 2019. Long-term mean, interannual and seasonal circulation in the Gulf of Finland – The wide salt wedge estuary or gulf type ROFI. *Journal of Marine Systems*, **195**, 1–19. DOI: 10.1016/j.jmarsys.2019.03.004.

Medvedev, I., A. Rabinovich and E. Kulikov, 2013. Tidal oscillations in the Baltic Sea. *Oceanology*, **53**, 526–538. DOI: 10.1134/S0001437013050123.

Muchowski, J., M. Jakobsson, L. Umlauf, L. Arneborg, B. Gustafsson, P. Holtermann, C. Humborg and C. Stranne, 2023. Observations of strong turbulence and mixing impacting water exchange between two basins in the Baltic Sea. *Ocean Science*, **19** (6), 1809–1825. DOI: 10.5194/os-19-1809-2023.

Palmén, E., 1930. Untersuchungen über die Strömungen in den Finnland umgebenden Meeren (Studies on the currents in the seas surrounding Finland). *Soc. Sc. Fenn., Comm. Phys.-Math.*, **12**. (in German).

Pavelson, J., 2005. "Mesoscale physical processes and the related impact on the summer nutrient fields and phytoplankton blooms in the western Gulf of Finland". PhD Thesis. Tallinn University of Technology.

Rasmus, K., M. Kiirikki and A. Lindfors, 2015. Long-term field measurements of turbidity and current speed in the Gulf of Finland leading to an estimate of natural resuspension of bottom sediment. *Boreal Environment Research*, **20**, 735–747. DOI: 10.60910/sbdt-6agn.

Salm, K., G. Väli, T. Liblik and U. Lips, 2025. Forcing-dependent submesoscale variability and subduction in a coastal sea area (Gulf of Finland, Baltic Sea). *Ocean Science*, **21** (5), 2555–2577. DOI: 10.5194/os-21-2555-2025.

Suhhova, I., T. Liblik, M.-J. Lilover and U. Lips, 2018. A descriptive analysis of the linkage between the vertical stratification and current oscillations in the Gulf of Finland. *Boreal Environment Research*, **23** (1–6), 83. DOI: 10.60910/kqwm-4rrc.

Suhhova, I., J. Pavelson and P. Lagemaa, 2015. Variability of currents over the southern slope of the Gulf of Finland. *Oceanologia*, **57** (2), 132–143. DOI: 10.1016/j.oceano.2015.01.001.

Suursaar, U. and R. Aps, 2007. Spatio-temporal variations in hydro-physical and -chemical parameters during a major upwelling event off the southern coast of the Gulf of Finland in summer 2006. *Oceanologia*, **49**, 209–228.

Symonds, D. R., 2006. QA/QC Parameters for Acoustic Doppler Current Profilers. *Teledyne RDI Application Note*. (last access: 3 Nov 2025). URL: https://content.aodn.org.au/Documents/IMOS/Quality_control/Working_group/ADCP/Teledyne-RDI_QAQC-Parameters-for-ADCPs.pdf.

Teledyne RD Instruments, 2011. *Acoustic Doppler Current Profiler Principles of Operation, A Practical Primer*. Teledyne RD Instruments A Teledyne Technologies Company.

Väli, G., V. Zhurbas, U. Lips and J. Laanemets, 2017. Submesoscale structures related to upwelling events in the Gulf of Finland, Baltic Sea (numerical experiments). *Journal of Marine Systems*, **171**, 31–42. DOI: 10.1016/j.jmarsys.2016.06.010.

Westerlund, A., L. Tuomi, P. Alenius, E. Miettunen and R. E. Vankevich, 2018. Attributing mean circulation patterns to physical phenomena in the Gulf of Finland. *Oceanologia*, **60** (1), 16–31. DOI: 10.1016/j.oceano.2017.05.003.

Westerlund, A., L. Tuomi, P. Alenius, K. Myrberg, E. Miettunen, R. E. Vankevich and R. Hordoir, 2019. Circulation patterns in the Gulf of Finland from daily to seasonal timescales. *Tellus A: Dynamic Meteorology and Oceanography*, **71** (1), 1627149. DOI: 10.1080/16000870.2019.1627149.

Witting, R., 1908. Untersuchungen zur Kenntnis der Wasserbewegugen und der Wasserumsetzung in den Finland umgebenden Meeren. *Finnländische Hydrograpisch-Biologische Untersuchungen*, **2**, 173.

Witting, R., 1910. *Rannikkomeret*. in Finnish.

Witting, R., 1912. *Zusammenfassende Übersicht der Hydrographie des bottnischen und finnischen Meerbusens und der Nördlichen Ostsee : nach den Untersuchungen bis Ende 1910*. 7. (last access: 3 Nov 2025) (in German). URL: https://www.doria.fi/handle/10024/171912.

Zhurbas, V., J. Laanemets and E. Vahtera, 2008. Modeling of the mesoscale structure of coupled upwelling/downwelling events and the related input of nutrients to the upper mixed layer in the Gulf of Finland, Baltic Sea. *Journal of Geophysical Research: Oceans*, **113** (C5). DOI: 10.1029/2007JC004280.

Appendix A. *ADCP info details*

Table A1: The ADCP moorings included in the dataset. The given depth is the depth measured during the deployment of the ADCP. †Deployed 10 meters from the seafloor, using 600 kHz ADCP.

Name	ID	Measurement period	Location	Depth of the measurement site
ADCP1	ADCP1_09	14 Apr – 09 Oct 2009	60° 04.077' N, 25° 27.068' E	52 m
	ADCP1_10	19 May – 21 Oct 2010	60° 04.077' N, 25° 27.068' E	51 m
	ADCP1_11	27 Jul – 21 Oct 2011	60° 04.077' N, 25° 27.068' E	51 m
	ADCP1_12	11 May – 09 Oct 2012	60° 04.000' N, 25° 25.590' E	52 m
	ADCP1_13	11 Apr – 16 Oct 2013	60° 04.000' N, 25° 25.600' E	51 m
	ADCP1_13b†	16 Oct 2013 – 01 Apr 2014	60° 04.000' N, 25° 25.617' E	51 m†
	ADCP1_14	01 Apr – 15 Oct 2014	60° 04.000' N, 25° 25.590' E	51 m
	ADCP1_14b	15 Oct 2014 – 24 May 2015	60° 04.000' N, 25° 25.617' E	51 m
ADCP2	ADCP2_09	16 Apr – 9 Oct 2009	59° 57.667' N, 25° 11.162' E	64 m
	ADCP2_10	19 May – 20 Sep 2010	59° 57.699' N, 25° 11.151' E	64 m
	ADCP2_11	02 Jun – 16 Sep 2011	59° 57.650' N, 25° 11.000' E	65 m
	ADCP2_12	07 May – 15 Nov 2012	59° 57.630' N, 25° 10.851' E	65 m
	ADCP2_13	11 Apr – 16 Oct 2013	59° 57.630' N, 25° 10.851' E	64 m
	ADCP2_13b	16 Oct 2013 – 01 Apr 2014	59° 57.630' N, 25° 10.851' E	64 m
	ADCP2_14	01 Apr – 14 Oct 2014	59° 57.634' N, 25° 10.873' E	63 m
	ADCP2_14b	14 Oct – 27 Dec 2014	59° 57.634' N, 25° 10.873' E	64 m
ADCP3*	ADCP3_09	14 Apr – 8 Oct 2009	59° 52.765' N, 25° 36.327' E	60 m
	ADCP3_10	20 May – 21 Oct 2010	59° 52.775' N, 25° 36.441' E	67 m
ADCP3	ADCP3_12	10 May – 31 Oct 2012	59° 54.989' N, 25° 33.560' E	71 m
	ADCP3_13	12 Apr – 16 Oct 2013	59° 55.000' N, 25° 33.530' E	71 m
	ADCP3_13b	16 Oct 2013 – 01 Apr 2014	59° 54.989' N, 25° 33.560' E	71 m
	ADCP3_14	01 Apr – 18 Dec 2014	59° 55.000' N, 25° 33.530' E	71 m
	ADCP3_14b	18 Dec 2014 – 24 May 2015	59° 55.000' N, 25° 33.530' E	71 m

Table A2: Notes on the deployment and quality issues. This information is also written in the data file headers in the `Notes` section (see Table 2.2).

File ID	Note
ADCP1_09	Installed to banana buoy, larger variations in heading and tilt. Uppermost bin data removed after 8 Aug 2009.
ADCP1_10	Higher number of missing data at bins 1–5, strong echo at these levels in beams 1 and 3.
ADCP1_13b	Deployed 10 meters from the seafloor. Large number of missing data at uppermost 10 bins. Ice disturbed measurements at the upper half of the water column during February.
ADCP1_14	Higher number of missing data at bins 1–10, strong echo at these levels in beams 1, 2 and 3.
ADCP2_10	Cells of missing data at bins 30–53 (around seasonal thermocline) from June to mid July 2010 rejected mainly by PG checks
ADCP2_12	Uncertainly in deployment depth. Slightly higher number of missing data after mid Septh 2012, mainly rejected by PG checks.
ADCP2_13	Cell of missing data around bin 40. Rejected by PG and error velocity checks
ADCP2_13b	Pressure sensor did not work. During Feb–Mar 2014 there are short instances where most of the measurements in the water column are rejected by all quality checks.
ADCP2_14b	Some cells of missing data around bins 30–40. Larger number of missing data at the uppermost 10 bins after December 2014. Data is rejected by all quality checks
ADCP3_09	Pressure sensor did not work.
ADCP3_10	Unclear measurement depth – clear error in metadata depth, determined based on ADCP measurements.
ADCP3_12	Depth measurements start to drift during July 2012. Depth values are marked as nan after 28.6.2012. Cells of missing data between mid May and mid June around bins 45–55 Missing measurements at upper most bins during day after mid Sept 2012. Data rejected by all quality checks
ADCP3_13	Pressure sensor did not work. Missing data around bins 40–55 most notably between mid May to early July. Data was rejected by all quality checks.
ADCP3_13b	During mid Jan–Mar 2014 there are short instances where most of the measurements in the water column are rejected by all quality checks.
ADCP3_14	Higher number of missing data at bins 1–12, strong echo at these levels in beams 1 and 3. Cells of missing data in Aug 2014 around bins 30–55. Increased amount of missing data at the uppermost layer in Dec 2014. Data is rejected by all quality checks.
ADCP3_14b	Pressure sensor did not work. Large number of missing measurements from uppermost 20 bins until Mar 2015. Data is rejected by all quality checks.